Communication Establishment Based on Authenticating Earprints

Sarah Othman Ali   Dr. Raid Rafi Omar Al-Nima   Dr. Emad Ahmed Mohammed

Technical Engineering College / Northern Technical University /

Mosul / Iraq

Email: sara_o_ali@ntu.edu.iq

ABSTRACT

Security systems widespread and play essential roles in our lives. The strongest security systems can be built by biometric traits. Earprint can be considered as one of the most important biometrics, especially for phone communications. In this paper, preprocessing steps are adopted for segmenting the used image and extracting its earprint pattern. In addition, a Deep Learning (DL) model has been suggested for personal verification. It is called the Normalized Deep Earprint Learning (NDEL). Furthermore, a communication prototype has been designed to analyze an earprint, then, provide a secure mobile phone call. The Earprint Image of Northern Technical University (EINTU) database has been utilized. Efficient preprocessing steps are successfully suggested for segmenting earprints. The results show that the NDEL achieved 98.0% and 99.7% for recognizing persons by using their employed left and right earprint patterns, respectively. Finally, secure mobile phone calls are achieved by utilizing earprint authentications.

Keywords: Biometrics, Mobile Phone Communications, Earprint, Deep Learning

1. Introduction

Over hundreds of years, humans have used their traits such as the face and voice to be essential resources for distinguishing each other. Several applications have utilized unique biometric traits/characteristics. One of the classical examples is security. Biometric have become a central issue in security for recognizing persons. Using personal biometric characteristics in security techniques can provide strongest systems.

Biometrics can generally be categorized into two types as reported and defined [1]:

1. Behavioral: this type of biometric refers to the behavioral styles of individuals. Examples of the of different behavioral biometric are signature [2], keystroke [3], gait [4] and voice [5].
2. Physiological: this type of biometric refers to the physiological characteristics within the bodies of persons. Example of such traits are fingerprint [6], face [7][8], irisprint [9][10], finger texture [11][12] and earprint [13].

Earprint is an attractive biometric characteristic, especially for communication purposes. This is mainly due to its pattern which is created during the pregnancy and it stays permanent after the born. Earprint patterns differ between people, twins, identical twins [14] and even between the right and left ears [15]. Therefore, it is difficult to find two ears that are totally identical. In addition, earprint has all the properties that make it efficient to be a biometric (i.e. permanence, universality, uniqueness and collectability

[16]). It is also not affected by expressions, feelings and emotions as other biometrics (e.g. face). Furthermore, the earprint pattern can easily be recognized by using low resolution and uncostly-acquisition device.

The human's external ear structure is relatively complicated; it has different features that construct unique earprint patterns. These features are the helix rim, antihelix, lobule, antitragus, tragus, crus of helix, triangular fossa, incisure intertragica and concha.

The contributions of the study can be illustrated as follows:

1. Efficient preprocessing steps are suggested for segmenting earprint images. They are adopted for images of right and left earprints in the Earprint Image of Northern Technical University (EINTU) database[17].
2. Proposing an effective Deep Learning (DL) model termed the Normalized Deep Earprint Learning (NDEL) network for verifying individuals based on their earprint patterns.
3. Suggesting an earprint authentication prototype for secure mobile phone communications, where a Global System for Mobile communications\General Packet Radio Service (GSM/GPRS) is used.

The remaining sections of the paper are organized as follows: the literature review is presented in Section 2, the segmentation of earprint images is described in Section 3, the NDEL model is illustrated in Section 4, the designed prototype for authenticated communication is presented in section 5, the experimental results are discussed in Section 6 and the conclusion of this study is given in Section 7.

2. Literature Review

Due to its singularity and individuality, various studies focused on earprint recognition. In 2000, Burge and Burger proposed automated earprint recognition. The authors offered a technique for localized the earprint in the image by using deformable contours. A series of edge detection and curve detection schemes were utilized to build a graph model of the earprint. Finally, the similarity of earprints can be achieved by a graph matching scheme [18]. It seems to be in this study only few sample of earprint was utilized. In 2006, Yan and Bowyer used contour information for earprint recognition. Three-Dimensional (3D) earprint images were exploited. This was the first study that considered the Principal Component Analysis (PCA) for 3D earprint images. A large experimental database was utilized, which provided the ability to explore several algorithms. The employed images were in Two-Dimensional (2D) and 3D [19]. Working on only left side of faces and employing various numbers of earprint images for each person can be considered as the main problem here. In 2012, Al-Nima suggested an earprint authentication system for telephone security purposes. Image preprocessing steps were applied for extracting the earprint features. These steps were: cropping, resizing, taking into account the three channels of (red, green and blue), dividing each image into blocks and computing the Mean Absolute Deviation (MAD) values of each block. Consequently, a probabilistic neural network was used for recognition. A total of 200 earprint images were utilized [13]. The database of this work is not available. In 2013, F. N. Sibai et al. used the artificial neural networks of feed-forward for earprint recognition. The authors identified seven features in 51 earprint images for different persons. Then,

many experiments were implemented for selecting the appropriate neural network by investigating different numbers of layers and neurons. The final result was achieved by utilizing the neural network with simple architecture that has three layers and 18 neurons in total [20]. The drawback of this work can be represented by using the small number of earprint images in a private employed database. In 2016, L. Tian et al. presented an earprint approach based on the CNN. The applied earprint database was from the University of Science and Technology Beijing (USTB-III). It included side-face images that show angle changes and hair occlusion [21]. A few images per subject were taken for only the right side of faces. In 2019, Ž. Emeršič et al. introduced a set of processes for earprint recognition. Earprint detection was performed by utilizing an end-to-end DL based Refinement (Refinet) model. Earprint feature extraction was manually done. Earprint recognition was employed by applying the Residual Neural Network (ResNet). The databases that used in this study were from the Unconstrained Ear Recognition Challenge (UERC) and the Annotated Web Ears (AWE) [22]. The weakness of this study can be represented by the used databases that collected from a website. These databases were not designed specifically for earprints. They contain inappropriate and low-quality earprint views, in addition to unequal number of images for each subject. In 2020, Jiang et al. presented and described the Deep Constellation Model for Ear (COM-Ear). Here, the deep constellation model was introduced for earprint recognition. The design was based on Siamese architecture. In this architecture, the earprint image was considered as global and its sub-images from a fixed grid of matrices were counted as locals. Global and local images were used as inputs to the COM-Ear model to generate the earprint representation at the output. In addition, a pooling operation named the Patch-Relevant-Information pooling (PRI-pooling) was introduced, it integrates features from the locals into the COM-Ear model. Extended Annotated Web Ears (AWEx) database was used for evaluating the suggested model. This database was collected from the web, so, it contains too many images. Various numbers of images per person were utilized [23]. Again, this database is not specifically established for earprints. Therefore, it has low-quality and inappropriate earprint views.

In this paper, a segmentation algorithm for earprint images is suggested and implemented. Fundamentally, a prototype is designed to establish secure mobile phone calls. Also from the literature, it can be noticed that only [23] considered the DL technique for earprint patterns. So, another significant contribution in this study is proposing an earprint DL model called the NDEL.

3. The Segmentation of Earprint Images

The EINTU images covers the earprint with the surrounded area of hair and skin. Extracting the earprint from a fully acquired image is not a straightforward process. An efficient algorithm is adopted to segment the earprint, isolate its Region of Interest (ROI) and prepare it for the next stage, see Fig. 1.

Multiple image pre-processing operations are suggested in this work as follow:

1. Converting the colored earprint channels (Red, Green and Blue (RGB)) into the 8-bits (grayscale) image. Assuming that the grayscale earprint image is defined as $E(x, y): \mathbb{Z}^2[0, 255]$.
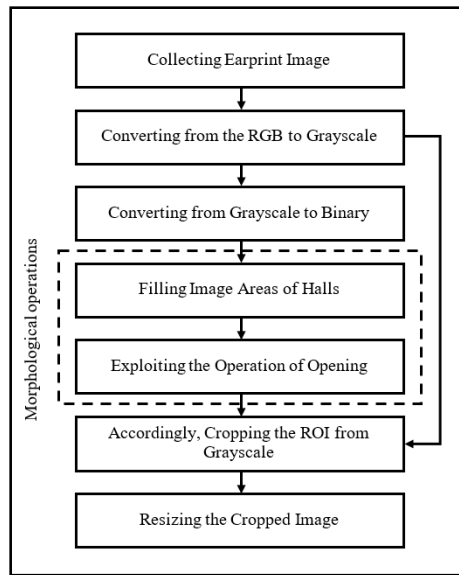
Figure 1: Adopted pre-processing operations

2. Transforming the $E(x, y)$ to a binary image (binarization) by employing the Otsu threshold. The general equation of changing an image from grayscale to binary is given as follows:

$$EB(x,y) = \begin{cases} 1 \text{ if } E(x,y) \geq Thr \\ 0 \text{ if } E(x,y) < Thr \end{cases} \qquad (1)$$

where $EB(x, y)$ is the binary image and Thr is the employed threshold. In this case, the adaptive threshold is utilized. To illustrate this, estimating a threshold according to Otsu is normally includes histogram analysis where its value automatically changes as follows:

   a- choosing a starting value for the Thr, the average intensity of the image is a good initial.

   b- computing the mean greyscale values μe_1 and μe_2 for the $E_1(x, y)$ and $E_2(x,y)$, where $E_1(x, y)$ and $E_2(x,y)$ represent the $E(x, y)$'s foreground and background, respectively.

   c- dividing the resulted image into two sets of $E_1(x, y)$ and $E_2(x,y)$ according to the value of Thr.

   d- determining a new threshold according to the following equation:

$$Thr = \frac{(\mu e_1 + \mu e_2)}{2} \qquad (2)$$

   e- repeating steps b to d until the mean values μe_1 and μe_2 in successive iterations stay the same [24].

3. Removing noises by applying morphological operations. These types of operations deal with binary images. In a morphological operation, each pixel in a binary image is adjusted according to the arranged values of its neighborhood pixels [25]. Filling small holes in the binary image $EB(x, y)$ and then performing the opening morphological process appear to be appropriate. In this way, the ROI of an earprint can be determined. Filling operation paints black holes inside white area by simply changing their values from logic zeros to logic ones [26]. It has the capability to remove small undesired noises inside a certain area. Opening operation is represented by erosion followed by dilation. Firstly, erosion reduces the size of white area by eliminating its border including surrounded noises. The formula of erosion can be expressed as follows:

$$A \ominus B = \{z \mid (B)_z \subseteq A\} \qquad (3)$$

where $\ominus$ is the mathematical representation of erosion morphological operation, $\mathbf{A}$ is a binary image, $\mathbf{B}$ is a structuring element of a designed binary pixels shape and $\mathbf{z}$ is a movable block of pixels in the binary image.

Secondly, dilation increases and preserves the overall size of white area. The equation of dilation can be represented as follows:

$$\mathbf{A} \oplus \mathbf{B} = \{\mathbf{z} \mid (\widehat{\mathbf{B}}) \cap \mathbf{A} \neq \emptyset\} \tag{4}$$

where $\oplus$ is the mathematical representation of dilation morphological operation, $\widehat{\mathbf{B}}$ is the symmetry of $\mathbf{B}$ and $\emptyset$ is the empty set.

In general, the opening operation smoothers the contour, breaks narrow isthmuses and eliminates thin protrusions of an object. The fully opening formula is as follows:

$$\mathbf{A} \circ \mathbf{B} = (\mathbf{A} \ominus \mathbf{B}) \oplus \mathbf{B} \tag{5}$$

where $\circ$ is the mathematical representation of opening morphological operation. This equation gives the relationship between erosion and dilation for performing the opening operation [27].

As a result of this step, the ROI of an earprint can be determined.

4. Cropping the grayscale image $E(x, y)$ according to the specified ROI. In other words, segmenting the ROI of the earprint from an input image.
5. Resizing the resulted image as this is required for the next stage of DL processes.

4. The NDEL Model

For the feature extraction and recognition stages, a DL model is suggested. Which it is called the NDEL. This model is based on the network architecture of a novel Deep Finger Texture Learning (DFTL) and Deep Earprint Learning which was approached in [11] and [17]. NDEL layers are sequentially composed of batch normalization, convolution, Rectified Linear Unit (ReLU), pooling, cross-channel normalization, fully connected, softmax and classification layers. Because of the simple descriptions of earprint patterns, there is no repetition in the first essential layers of Convolutional Neural Network (CNN) [28]. The architecture of the presented NDEL model is given in Fig. 2.
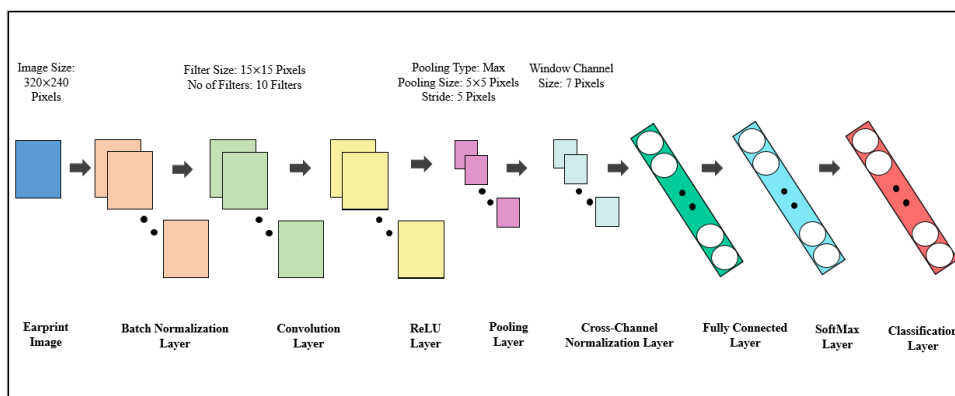

Figure 2: The architecture of the presented NDEL model

Each layer in the NDEL network can be described as follows:

4.1 Batch normalization layer:

The batch normalization layer independently normalizes for each channel a batch of data across all observations (values). This layer normalizes the values of the input image **IM** by firstly calculating the variance σ^2 and mean μ over the spatial and observation dimensions. Then, the normalized activation function is calculated as follows:

$$IMB_{row,col} = \frac{IM_{row,col} - \mu}{\sqrt{\sigma^2 + \epsilon}} \tag{6}$$

where $IMB_{row,col}$ is a batch normalization layer outcome, row is the number of rows, col is the number of columns and ϵ is a constant, it enhances numerical stability when the σ^2 is too small. Allowing for the possibility of μ and σ^2 that are not appropriate for the operations of batch normalization as μ equal to zero, the batch normalization operation further shifts and scales the activation function values using the following equation:

$$IMB_{row,col} = \beta + \gamma IMB_{row,col} \tag{7}$$

where β is the offset shifting and γ is the scale factor. Both of these parameters are learnable, in which they are updated during the training phase [29].

4.2 Convolution layer:

The convolution layer produces feature maps that are extracted from each channel c_{in} of the previous layer (c_{in} here equals to 1 as the input earprint image is of a greyscale type). The feature map represents a convolved c_{in} with a kernel (a set of weights). Generally, the kernel has a size of $k_w \times k_h \times c_{in}$ pixels. Fundamentally, k_w and k_h represent the kernel width and height, respectively. The main equation of the convolution layer is given as follows:

$$O_{z,t,q} = B_q + \sum_{i=1}^{c_{in}} \sum_{j=1}^{k_h} \sum_{k=1}^{k_w} IMB_{zS+j,tS+k'i} \times W_{j,k,i,q} \tag{8}$$

where $O_{z,t,q}$, B_q, $IMB_{zS+j,tS+k'i}$ and $W_{j,k,i,q}$ are an outcome of the convolution layer for a specific pixel coordination of (z,t) in channel q, a bias, an input from the previous layer and a kernel value, respectively. The number of activation maps pixels that the kernel is shifted after every single convolution is defined as S [30].

4.3 ReLU layer:

In this layer, a ReLU activation function is employed. The advantage of this layer is to provide a non-linear computation by keeping the positive values and removing the negative values from the feature maps. The ReLU activation function calculation is given by the following equation:

$$y_{z,t,q} = f(O_{z,t,q}) = \max(0, O_{z,t,q}) \tag{9}$$

where an outcome of the ReLU layer is represented by $y_{z,t,q}$ and **max** stands for the maximum operation [31].

4.5 Pooling layer:

The pooling layer performed a necessary role in decreasing the sizes of received channels. The pooling layer extracts maximum or average values from the resulted ReLU outcomes. Here, it decreases the sizes of the obtained features by collecting maximum values. The general equation of the maximum pooling layer is as follows:

$$p_{a^l,b^l,c} = \max_{0 \le a < h_p, 0 \le b < w_p} y_{a^l \times h_p + a, b^l \times w_p + b, c} \tag{10}$$

where a pooling layer outcome is $p_{a^l,b^l,c}$, $0 \le a^l < h_p^l$, h_p^l is the height of a pooled channel, $0 \le b^l < w_p^l$, w_p^l is the width of a pooled channel, $0 \le c < c^l = c^{l-1}$, l and l-1 are respectively refer to the current layer and previous layer, and w_p and h_p respectively

represent the width and height of a sub-region that need to be pooled from ReLU outcomes [32].

4.6 Cross-channel normalization layer:

The cross-channel normalization layer provides channel-wise local response normalization. This layer is known as brightness normalization. For each input from pooling layer the normalized activation function $lrn_{a^l,b^l,c}^{ir}$ is given by:

$$lrn_{a^l,b^l,c}^{ir} = \frac{p_{a^l,b^l,c}^{ir}}{\left(kr + ar\sum_{jr=\max(0,ir-\frac{nr}{2})}^{\min(NR-1,ir+\frac{nr}{2})}\left(p_{a^l,b^l,c}^{jr}\right)^2\right)^{\beta r}} \tag{11}$$

where ir is the applied kernel, nr is the adjacent kernel maps for a certain spatial position, NR is the total number of kernel maps in the layer, and the constants kr, ar and βr are hyper-parameters☐ [29].

4.7 Fully connected layer:

The fully connected layer is for mapping between the previous layer and a certain number of neurons. It can effectively map between both the pooling layer and the required number of classes or subjects (outputs). The operation of the fully connected layer is given in Equation (7) as follows:

$$FC_r = \sum_{d=1}^{mc_1^{l-1}}\sum_{g=1}^{mc_2^{l-1}}\sum_{h=1}^{mc_3^{l-1}} W_{d,g,h,r}^l(\mathbf{lrn}_c)_{d,g} \,\forall 1 \leq r \leq mc^l \tag{12}$$

where a fully connected layer outcome is FC_r, the width and height of a pooling layer channel are mc_1^{l-1} and mc_2^{l-1}, the number of created channels in the pooling layer is mc_3^{l-1}, a connected weight value between the previous layer and the fully connected layer is $W_{a,b,c,r}^l$, the channel-wise local response (cross-channel) normalization layer outcomes is $\mathbf{lrn}_c$, and the number of required neurons in the current layer (it can be equal to the number of required classes or outputs) is mc^l [24].

4.8 Softmax layer:

The softmax activation function is used to calculate the classification probabilities for each input image. It can be represented by the following equation:

$$SO_r = \frac{e^{FC_r}}{\sum_{s=1}^{mc^{l-1}} e^{FC_s}}, \quad r=1, 2, \ldots, mc^l \tag{13}$$

where a softmax layer outcome is SO_r [24].

4.9 Classification layer:

The classification layer is utilized at the end for achieving the final decision of recognition or classification. The rule in this layer is known as the winner-takes-all. The equation of this layer can be represented as follows:

$$CL_r = \begin{cases} 1 & \text{if } SO_r = \text{Max} \\ 0 & \text{otherwise} \end{cases}, \quad r=1, 2, \ldots, mc^l \tag{14}$$

where an output decision of this layer is CL_r and $\mathbf{Max}$ is the obtained maximum value from the softmax layer [33].

The outputs of the NDEL model can be considered as multi-classes. Since the multi-classes can be used for the verification according to [33] [34], the NDEL has been adopted for individual verification based on the earprint. Depending on the NDEL outputs, multi-classes of certain subjects can be verified.

☐ Default values for constant parameters: $kr = 2$, $nr = 5$, $ar = 10^{-4}$ and $\beta r = 0.75$.

5. The Designed Prototype for Authenticated Communication

This section describes the authenticated communication hardware requirements to provide phone calls, the previously described headset with microphone, speaker and camera, personal computer, Arduinos, GSM\GRPS, voltage regulator□, and mobile phone are employed in a communication prototype as shown in Fig. 3.
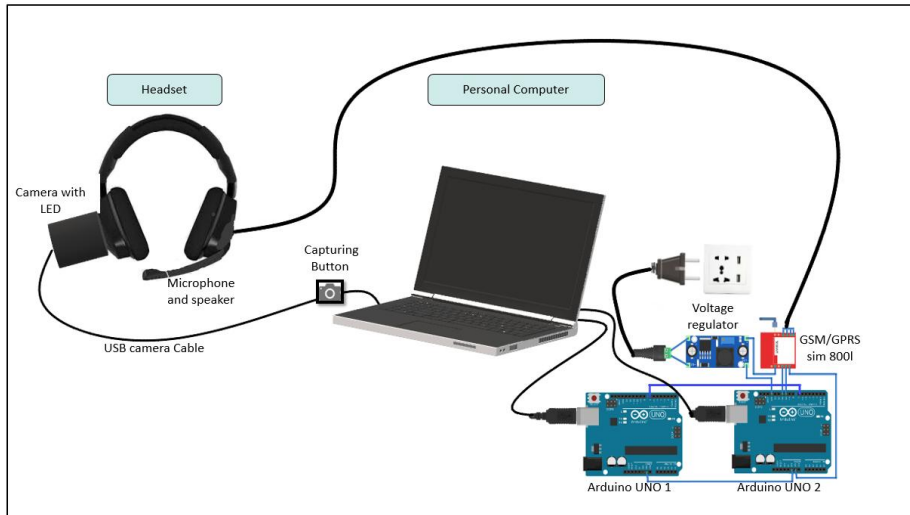

Figure 3: Hardware parts of designed communication prototype

The main authenticated communication hardware parts (the Arduinos, GSM\GRPS, mobile phone, and microphone and speaker in a headset) can be described as follows:

5.1 Arduinos:

Arduino is an open-source microcontroller that allows a computer to be connected with an external device or even multiple external devices [35]. Components of an Arduino (type UNO) are shown in Fig 4 and they can be illustrated as follows [36]:

- External power supply: it is obviously used to power up the boar
- Reset button: it is utilized to reset the software program when it is pressed.
- Microcontroller: it is the brain of Arduino and it is here of type ATmaga 328P. It is in charge of executing the instructions.
- Analogue pins: these pins are assigned for inputting analogue information.
- Digital Input / Output (I/O) pins: these pins are determined for accepting digital information as the input or output.
- Ground pins: they are for the ground connection.
- Power pins: they are for supplying 3.3V and 5V.

This study utilizes two Arduinos of type UNO. The first and main one can be used as a phone switching to direct the communication into the appropriate GSM\GPRS, where many GSM\GPRSs are allowed to be utilized. This Arduino receives an order from the connected computer and transmits a command signal to the second or certain Arduino which is connected to the GSM\GPRS in order to make a phone call with a determined phone number. The second Arduino works as sub-controller for a GSM\GPRS and it is in charge of applying its phone calls.
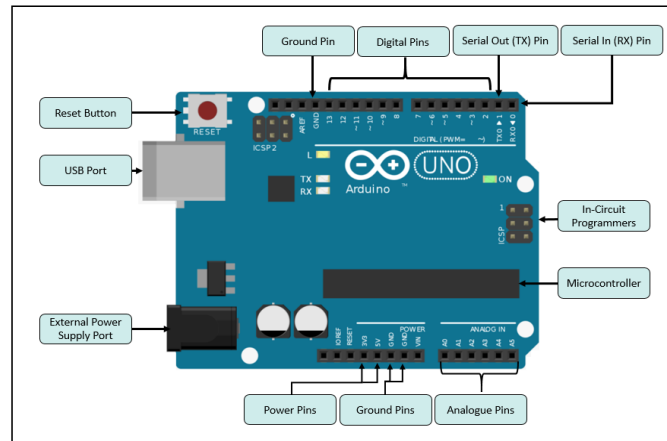

□ For regulating the GSM\GRPS power voltage.

Figure 4: Components of an Arduino of type UNO

5.2 GSM\GPRS:

GSM\GPRS is exploited for a digital and wireless mobile communications. It is of type Sim800l. This type is able to send and receive mobile phone calls, in addition to Short Message Service (SMS) messages [37]. Fig 5 demonstrates the GSM\GPRS of type Sim800l. When the power is connected to the GSM\GPRS, it starts searching for cellular networks. Then, it is automatically connected to an available wireless mobile network. The LED on the board shows a connection state, where the LED fast blinking refers to no network coverage and slow blinking refers to successfully logged in.

The Sim800l has two antennas.The first antenna has a helical shape, it is external and directly soldered to a Network status (NET) pin in the GSM\GPRS. This antenna is very useful for a good wireless coverage area. The second antenna is a Printed Circuit Board (PCB) which is connected to a cable that is conducted to the Internetwork Packet Exchange (IPX). This antenna can lead to better communication performance, where it gives more free indoor of using and allows putting the module inside a metal case.
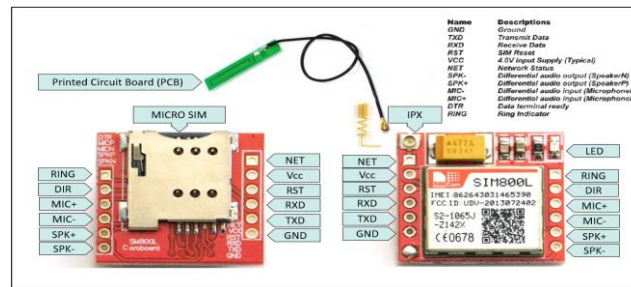

Figure 5: Demonstrating the GSM\GPRS of type Sim800l

The GSM\GPRS specifications of type Sim800l is as follows [37] [38]:

- Supplying voltage level between 3.8V to 4.4V.
- Power consumption in sleeping mode equals to 2.0mA and in idle mode equals to less than 7.0mA.
- Power consumption for the Global System for Mobile communications (GSM) transmission on average is 350mA (the peak transmission is 2000mA).
- The small size of 25cm✕23cm.
- Subscriber Identity Module (SIM) socket of type micro-SIM.

- Supported frequencies are quad bands of 850MHz, 950MHz, 1800MHz and 1900MHz.

In addition, it is very sensitive to the supplied voltage level as it may not work properly if the voltage level is high or low. The recommended supplied voltage is 4V. Therefore, a voltage regulator is exploited to exactly provide this voltage value. Moreover, it has a small size and it is considered an inexpensive.

This study utilizes the GSM\GPRS of type Sim800l that is used together with the Arduino, designed headset and laptop. By this package, mobile phone calls can be initiated for an authenticated earprint.

5.3 Microphone and Speaker:

The previously described acquisition headset system is modified by adding an external microphone and speaker. In order to connect the microphone to the GSM\GPRS, the positive wire of the microphone is soldered to the positive differential audio input pin and the negative wire of the microphone to the negative differential audio input pin. Similarly, in order to connect the speaker to the GSM\GPRS, the positive wire of the speaker is soldered to the positive differential audio output pin and the negative wire of the speaker to the negative differential audio output pin. Hereafter, the headset can transmit and receive audio signals via the GSM\GPRS.

5.4 Mobile cell Phone:

All types of mobile phone devices that use the GSM can be used for the suggested communications by authenticating earprint patterns. Even if the devices are for old mobile phones and smart mobile phones. In this study, several types of mobile phone devices are exploited as: Huawei Nova 3, Samsung Galaxy and HTC one.

6. The Experimental Results
6.1 Implementations of Pre-processing

The EINTU earprint image is passing through pre-processing operations in order to be ready for the DL stage. As detailed in section 3, the pre-processing operations follow an efficient adopted algorithm. Example of resulted implementations for each operation is as follows:

1. First of all, converting a colored image which is shown in Fig. 6 (a) to the grayscale image is resulted as given in Fig. 6 (b).
2. Applying the binarization to the grayscale image by using the Otsu threshold [24] is resulted as demonstrated in Fig. 6 (c).
3. Performing the fill morphological operation, see Fig. 6 (d). It can be noticed from this figure that all small black holes in the big white area have been deleted. Then, implementing the open morphological operation is resulted as shown in Fig. 6 (e). It can be seen from this figure that this operation removes the noises and provides an ROI region of the earprint.
4. Cropping the grayscale image that has been obtained from the first step according to the previous outcome of an ROI. In other words, segmenting the exploited earprint as given in Fig.6 (f).
5. Resizing the resulted image. So that all images have the same size since ROIs of earprints differ between images and people. In addition, image resizing is required for the next DL stage. It is suitably selected to get the size of 200×150 pixels, see Fig.6 (g).
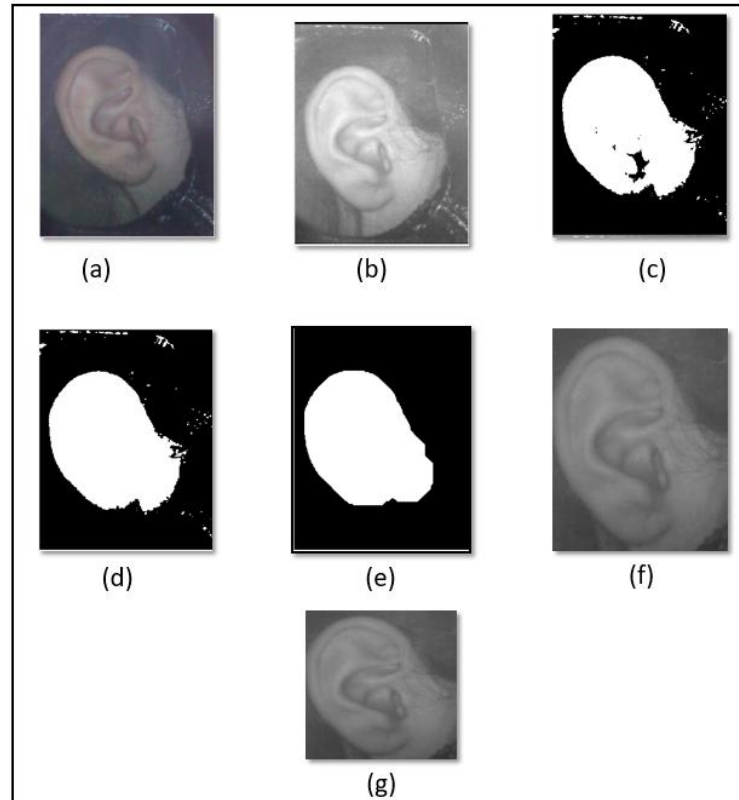
Figure 6: (a) An acquired colored image of an earprint pattern, (b) Resulted grayscale image of the acquired colored image, (c) Resulted binary image after applying the binarization, (d) Resulted image after the filling morphological operation, (e) Resulted image after the opening morphological operation, (f) Resulted earprint image after the segmentation and (g) Resulted earprint image after the resizing

6.2 NDEL Specifications

As mentioned earlier, a new DL model is proposed, it is called the NDEL. It is used for extracting earprint pattern features and providing personal verification performances. The input of NDEL is the EINTU database after pre-processing. Each input image has a size of 200×150 pixels. The output neurons of the NDEL are adapted to produce a verification result, where each subject is represented by an output neuron or a class. A similar idea is presented by [12][39]. In this work, 75 output neurons for 75 subjects have been determined where all volunteers have participated in the two acquisition sessions of collecting the EINTU database. The NDEL has separately been implemented for right ears and left ears. Overall, 20 earprints have been employed for each subject and a total of 3000 images have been used.

NDEL parameters are as follows: the filter size of the convolution layer is 15×15 pixels, the number of convolution layer filters is 10, pooling layer has been assigned to the maximum type, the pooling filter size is 5×5 pixels, the pooling stride is 5 pixels and the channel window size of the cross channel normalization layer is 7.

6.3 Computer Descriptions

NDEL training and testing implementations are applied in a computer with the following descriptions: LENOVO Laptop, Intel Core i7 processor, 2.20 GHz processor speed, 16 GB computer memory, NVIDIA display card, GeForce GTX 1060 graphics processor and 6 GB display memory.

6.4 NDEL Training

First of all, 50% of the employed images have randomly been collected and used in each of the training phases for right and left earprints (750 images for the right and 750 images for the left). Secondly, the NDEL network has been trained using the following parameters: Stochastic Gradient Descent with Momentum (SGDM) optimizer, momentum value of 0.9, fixed learning rate value of 0.0003, weight decay value of 0.0001, the mini-batch size value of 128 and maximum epoch of 100. Figs. 4.7 and 4.8 show how the training phases have succeeded for left and right earprint patterns, respectively. They clarify the accuracies and loss errors of mini-batches along with iterations.

It can be noticed that the accuracy was successfully increased in Fig. 7(a) and the error was reasonably decreased in Fig. 7(b) during the training process. Finally, the accuracy reached its maximum level and the error attained its minimum level.
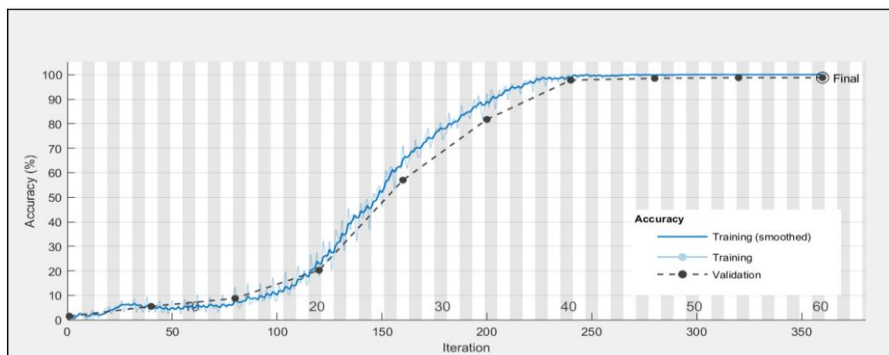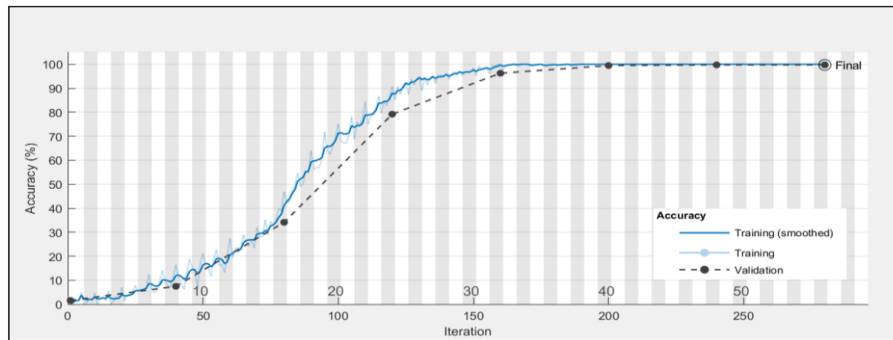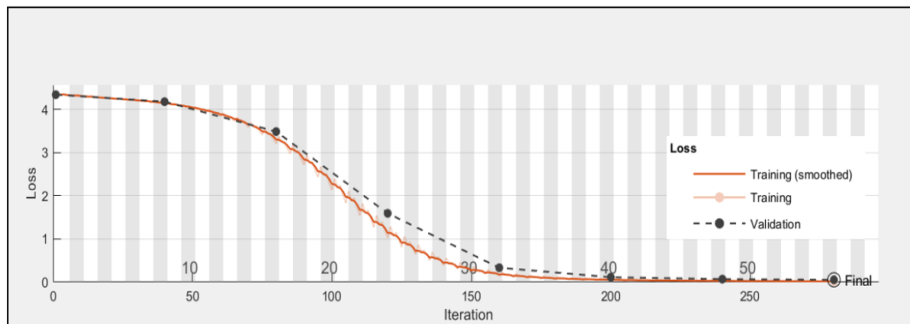

(a)
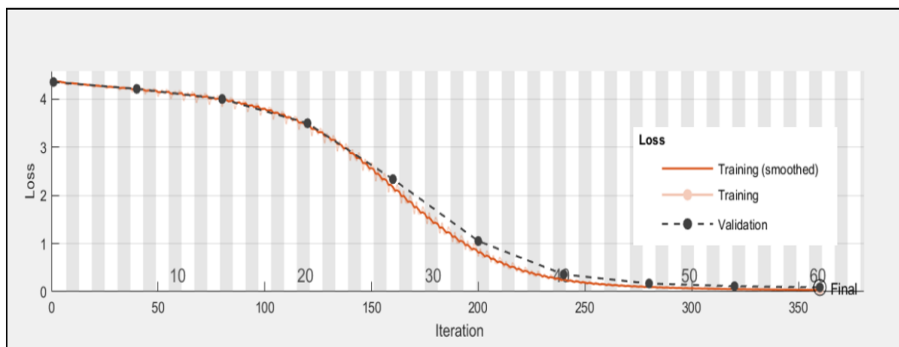
(b)

Figure 7: Training progress curves for left earprint patterns:(a) accuracy curve and (b) loss error curve

Similarly, it can be observed that the accuracy was correctly increased in Fig. 8(a) and the error was acceptably decreased in Fig. 8(b) during the training process. Finally, the accuracy attained its highest level and the error reached its lowest level.

(a)

(b)

Figure 8: Training progress curves for right earprint patterns:(a) accuracy curve and (b) loss error curve

6.5 NDEL Validation

Validation samples have randomly been collected and utilized in the training phases of right and left earprints too. They consider only 25% of the employed images for each of left and right earprint patterns (375 images for the right and 375 images for the left). Validation curves are shown in Figs. 4.9 and 4.10 within the train progresses. Applying validation samples has the following advantages: making the training evaluations more biased, indicating the end of a train and preventing the overfitted performances.
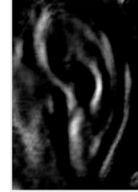
6.6 Earprint Feature Extraction

The NDEL consists of two main parts, these parts are feature extraction and classification. The feature extraction part involves the following layers: batch normalization layer, convolution layer, ReLU layer, pooling layer and cross-channel normalization layer. The classification part includes the following: fully connected layer, softmax layer and classification layer. Efficient and automatic feature extraction of earprint patterns can be obtained by the NDEL feature extraction layers. Tabl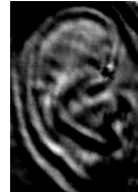e 1 demonstrates various validation samples of earprint patterns that are collected from the NDEL feature extraction layers.

In this table, it can be observed that an input earprint image is resulted in the batch normalization layer with no shown differences, however, the values are influenced by the normalization process. Then, the convolution layer can provide different appeared feature maps of earprints based on the kernel values that are automatically produced by the optimization algorithm. Subsequently, the ReLU layer discards all earprint features of

negative values and appears black color instead. Consequently, the pooling layer reduces the sizes of resulted earprint vectors from the previous layer. It preserves here the earprint features that have maximum values.

After that, the cross-channel normalization layer does not represent significant differences in appearances compared to the previous layer, however, it decreases the sensitivity of earprint images to brightness by normalizing the obtained values. Finally, it can be seen that earprint patterns are efficiently analyzed by the NDEL feature extraction layers.

Table 1: Various validation samples of earprint patterns which are collected from the NDEL feature extraction layers

Earprint samples	Input validation earprint images	Feature extraction in the batch normalization layers	Feature extraction in the convolution layers	Feature extraction in the ReLU layers	Feature extraction in the pooling layers	Feature extraction in the cross-channel normalization layers
Left earprint sample						
Right earprint sample						

6.7 NDEL Testing

For the testing phase, the remaining 25% of the employed images in each of right and left earprints have been exploited (375 images for the right and 375 images for the left). Earprint patterns of left and right ears are separately tested, each with its certain NDEL model.

Tables 2 shows the benchmarked verification accuracies and EERs for each of left and right earprint patterns.

Table 2: Benchmarked verification accuracies and EERs for each of left and right earprint patterns

Evaluated NDEL	Accuracy	ERR
NDEL for left earprints	98.0%	2.0%
NDEL for right earprints	99.79%	0.21%

From this table, it can be noticed that the obtained verification accuracy by the proposed NDEL model for left earprint images is 98.00%, where the attained ERR is

2.00%. Furthermore, the achieved verification accuracy by the same NDEL model for right earprint images is 99.79%, where the benchmarked ERR is 0.21%.

According to the results that are obtained from the testing process, it can be declared that both earprint patterns have attained comparable performances. So that, the left or right earprints may effectively be employed in any verification system.

6.8 Comparisons:

The NDEL has been compared with state-of-the-art architectures of DL networks. Several network models for the employed database are simulated and evaluated. These are the Deep Finger Texture Learning (DFTL) [11], X_axis Classification Model (XCM) [40], Z_axis Classification Model (ZCM) [41], Dual Deep Fingerphoto Learning (DDFL) [42], Y_axis Classification Model (YCM) [40] and Palm Convolutional Neural Network (PCNN) [43]. Comparison accuracies and EERs with state-of-the-art architectures of DL networks are given in Tables 3. From Table 3, it can be observed that the DFTL network architecture attained the accuracies of 85.73% and 90.91% for left and right earprints, respectively. The XCM, ZCM and YCM respectively achieved the results of 90.13%, 93.20% and 95.73% for left earprints. They also respectively obtained the results of 89.92%, 92.55% and 97.26% for right earprints. The DDFT reported performances of 95.20% and 97.14% for left and right earprints, respectively. The PCNN recorded the accuracies of 96.93% and 98.13% for left and right earprints, respectively. It is clear that the suggested NDEL has benchmarked the results of 98.00% and 99.79 % for left and right earprints, respectively.

Table 3: Comparison accuracies with state-of-the-art architectures of DL networks

References	DL Networks	Accuracies for left earprints	Accuracies for right earprints
OMAR ET AL. [11]	DFTL	85.73%	90.91%
AL-HATAB ET AL. [40] [41]	XCM	90.13%	89.92%
	ZCM	93.20%	92.55%
	YCM	95.73%	97.26%
AL-NIMA ET AL. [42]	DDFT	95.20%	97.14%
ALBAK ET AL. [43]	PCNN	96.93%	98.13%
PROPOSED APPROACH	NDEL	98.00%	99.79 %

To illustrate, the architectures of the DFTL, XCM, ZCM, YCM, DDFT and PCNN networks are constructed by specific layers with determined parameters. They are capable for verifying individuals according to their earprint patterns, however, their qualifications are not very suitable for such task. On the other hand, the architecture of the proposed NDEL network is more appropriate in analyzing earprint patterns and verifying the related persons.

6.9 Communication Establishment:

For establishing a human communication by authenticating his/her earprint pattern, the prototype presented in Chapter Three is implemented. MATLAB software instructions are utilized for the NDEL model and communication establishment by the first (main) Arduino. C++ software instructions are used for connecting the second Arduino with the GSM\GPRS.

To start or discard a secure mobile phone call, the following steps can be employed:

1. Capturing the earprint image by using the acquisition device.
2. Appling the segmentation algorithm.
3. Verifying the person by using the NDEL model.
4. If the person is successfully verified, he/she is authorized for establishing the mobile phone call:
   a. Sending a signal to the main Arduino (this Arduino can be used as a switch to direct the communication into the suitable GSM\GPRS) which order the second Arduino to establish a call via its GSM\GPRS.
   b. Starting the certain secure call with the specific mobile phone number.
5. Otherwise, if the person is not verified, he/she is not authorized for establishing the mobile phone call.
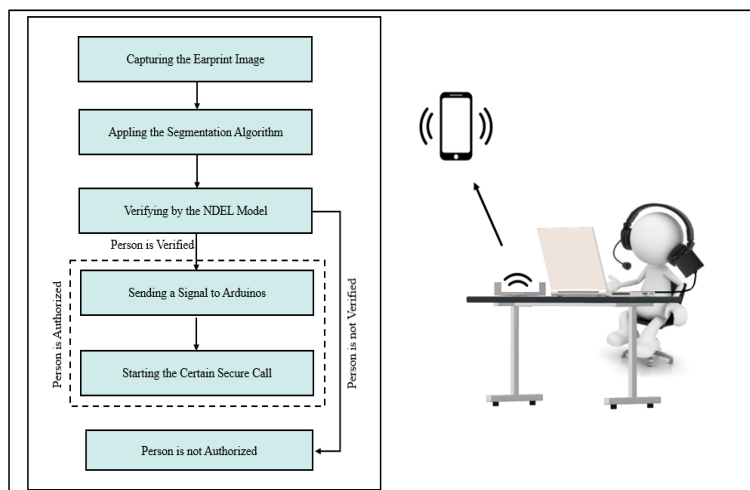

Figure 9: Block diagram for establishing a secure mobile phone call

The block diagram of these steps are shown in Fig. 9. Moreover, all the hardware components that are utilized in this work are given in Fig.10. The demonstration of a

mobile phone communication establishment by exploiting the earprint pattern is provided in Fig.11.
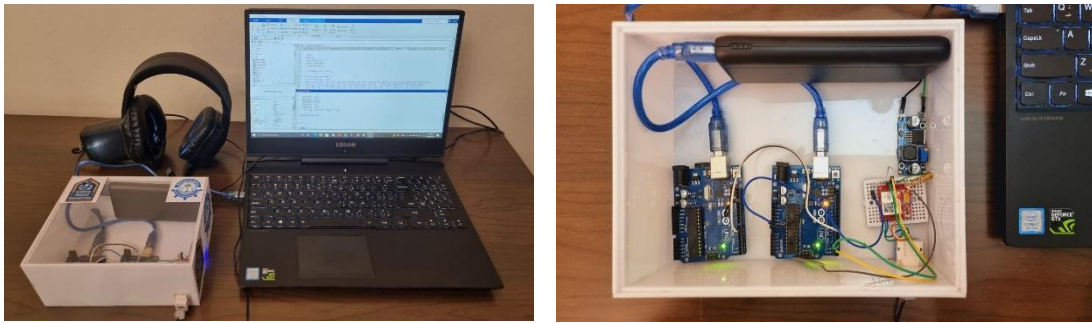
(a)

(b)

Figure 10: Hardware components that are utilized in this work
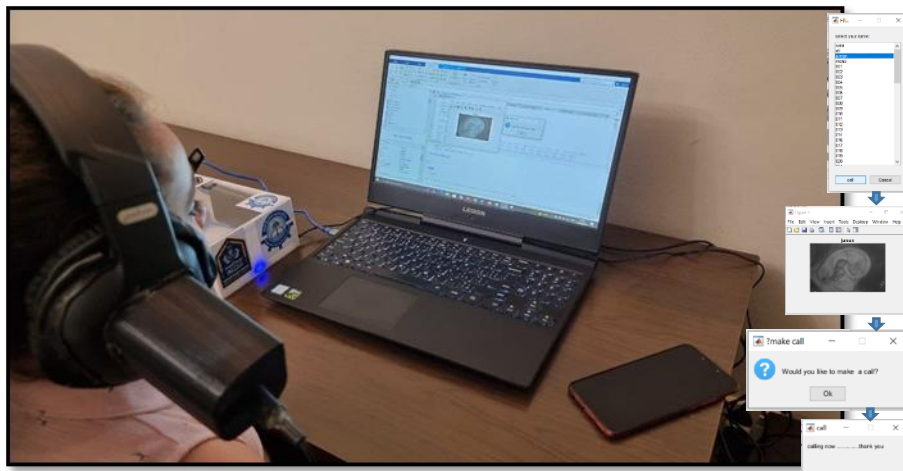
(a)

(b)

Figure 11: Demonstration of a mobile phone communication establishment by exploiting the earprint pattern

Both hardware and software parts can work together. In general, a person is firstly asked to wear the designed headset and select the appropriate options in the program,

including his/her verification information. The earprint image is captured, segmented and analyzed. A verification decision is provided. If the person is verified the program gives the authentication to establish the secure mobile phone call. As illustrated in last figure, the communication is successfully established.

The proposed methods can be counted with other confirmed techniques as in [44-68].

7. Conclusions

The conclusions of this paper can be expressed according to the presented work and obtained results as follows:

- Pre-processing operations on the acquired images were adopted to segment an earprint region.
- A deep learning model for feature extraction and verifying people by using their earprint patterns was proposed, which is called the NDEL. The architecture of the NDEL was reasonable to earprints as they have simple and reliable patterns. Earprint images from the EINTU database were applied to the suggested NDEL for both left and right ears in the case of personal verification.
- The main results were impressive and surpassed. That is, the accuracies were reported as 98.00% and 99.79% for left and right earprint patterns, respectively. Also, the EERs were recorded as 2.00% and 0.21% for left and right earprint patterns, respectively.
- It can be concluded that each of the left and right earprint patterns can be effectively utilized in secure verification and authentication systems.
- Using appropriate hardware components including Arduinos, GPS/GPRS, and mobile phones to establish secure communication connections based on authenticated earprint patterns. As a result, communication calls were successfully established.

References

[1] M. Bača, M. Schatten, and J. Ševa, "Behavioral and Physical Biometric Characteristics Modeling Used for Its Security Improvement", *Transport Problems*, Vol. 4, No. 4, p. 9, 2009.

[2] R. R. Al-Nima, S. Dlay, and W. Woo, "A new approach to predicting physical biometrics from behavioural biometrics", *International Journal of Computer, Information, Systems and Control Engineering*, Vol. 8, No. 11, 2014.

[3] Y. Zhong, Y. Deng, and A. K. Jain, "Keystroke Dynamics for User Authentication", *2012 IEEE Computer Society Conference on Computer Vision and Pattern Recognition Workshops*, pp. 117–123, 2012.

[4] M. Z. Uddin, W. Khaksar, and J. Torresen, "A robust gait recognition system using spatiotemporal features and deep learning", *IEEE International Conference on Multisensor Fusion and Integration for Intelligent Systems*, Vol. 2017-Novem, No. Mfi, pp. 156–161, 2017.

[5] Musab T. S. Al‐Kaltakchi, Raid Rafi Omar Al‐Nima, Mohammed A. M. Abdullah, and Hikmat N. Abdullah, "Thorough Evaluation of Timit Database Speaker Identification Performance Under Noise With and Without the G.712 Type Handset",

Springer, International Journal of Speech Technology, Vol. 22, No. 3, pp. 851–863, 2019.

[6] Abdulsattar M. Ibrahim, Abdulrahman K. Eesee, and Raid Rafi Omar Al-Nima, "Deep Fingerprint Classification Network", *TELKOMNIKA Telecommunication, Computing, Electronics and Control*, Vol. 19, No. 3, 2021.

[7] Raid Rafi Omar Al-Nima, Farqad Hamid Abdulraheem, and Moatasem Yaseen Al-Ridha, "Using Hand-Dorsal Images to Reproduce Face Images by Applying Back propagation and Cascade-Forward Neural Networks", *2nd International Conference on Electrical, Communication, Computer, Power and Control Engineering (ICECCPCE19)*, IEEE, Mosul, Iraq, 13-14 February, 2019.

[8] Raid Rafi Omar Al-Nima, Moatasem Yaseen Al-Ridha, and Farqad Hamid Abdulraheem, "Regenerating Face Images from Multi-Spectral Palm Images Using Multiple Fusion Methods", *TELKOMNIKA Telecommunication, Computing, Electronics and Control*, Vol. 17, No. 6, pp. 3120-3129, December 2019.

[9] M. A. M. Abdullah, R. R. Al-Nima, S. S. Dlay, W. L. Woo, and J. A. Chambers, "Cross-spectral Iris Matching for Surveillance Applications", *Springer, Surveillance in Action Technologies for Civilian, Military and Cyber Surveillance*, Chapter 5, 2017.

[10] Raid Rafi Omar Al-Nima, "Personal Identification Based on Iris Patterns", Master thesis, Technical Engineering College of Mosul, Iraq, 2006.

[11] R. R. Omar, T. Han, S. A. M. Al-Sumaidaee, and T. Chen, "Deep Finger Texture Learning for Verifying People", *IET Biometrics*, Vol. 8, Issue 1, 2019.

[12] M. T. Al-Kaltakchi, R. R. Omar, H. N. Abdullah, T. Han, and J. A. Chambers, "Finger Texture Verification Systems Based on multiple spectrum Lighting Sensors with Four Fusion Levels", *Iraqi Journal of Information & Communications Technology*, Vol. 1, No. 3, pp. 1–16, 2019, doi: 10.31987/ijict.1.3.28.

[13] R. R. Al-Nima, "Human Authentication with Earprint for Secure Telephone System", *Iraqi Journal of Computers, Communications, Control and Systems Engineering IJCCCE*, Vol. 12, No. 2, 2012.

[14] H. Nejati, L. Zhang, T. Sim, E. Martinez-Marroquin, and G. Dong, "Wonder ears: Identification of identical twins from ear images", *Proceedings - International Conference on Pattern Recognition*, No. February 2019, pp. 1201–1204, 2012.

[15] A. Abaza and A. Ross, "Towards understanding the symmetry of human ears: A biometric perspective", *IEEE 4th International Conference on Biometrics: Theory, Applications and Systems, BTAS 2010*, 2010.

[16] A. K. Jain, A. Ross, and S. Prabhakar, "An Introduction to Biometric Recognition", *IEEE Transactions on Circuits and Systems for Video Technology*, Vol. 14, No. 1, pp. 4–20, 2004.

[17] Sarah Othman Ali, Raid Rafi Omar Al-Nima, and Emad Ahmed Mohammed, "Individual Recognition with Deep Earprint Learning", *2021 International Conference on Communication & Information Technology (ICICT) - Basra - IRAQ*, 2021.

[18] M. Burge and W. Burger, "Ear biometrics in computer vision", *Proceedings - International Conference on Pattern Recognition*, Vol. 15, No. 2, pp. 822–826, 2000.

[19] Ping Yan and K. Bowyer, "Empirical Evaluation of Advanced Ear Biometrics", *In 2005 IEEE Computer Society Conference on Computer Vision and Pattern Recognition (CVPR'05)-Workshops*, pp. 41-41. IEEE, 2005.

[20] F. N. Sibai, A. Nuaimi, A. Maamari, and R. Kuwair, "Ear recognition with feed-forward artificial neural networks", *Neural Computing and Applications*, Vol. 23, No. 5, pp. 1265–1273, 2013.

[21] L. Tian and Z. Mu, "Ear recognition based on deep convolutional network", *Proceedings - 2016 9th International Congress on Image and Signal Processing, BioMedical Engineering and Informatics, CISP-BMEI 2016*, pp. 437–441, 2017.

[22] Ž. Emeršič, J. Križaj, V. Štruc, and P. Peer, "Deep ear recognition pipeline", *Studies in Computational Intelligence*, Vol. 804, pp. 333–362, 2019.

[23] D. Štepec, Ž. Emeršič, P. Peer, and V. Štruc, "Constellation-Based Deep Ear Recognition", *Deep biometrics*, pp. 161-190, Springer, Cham, 2020.

[24] N. Otsu, "A Threshold Selection Method From Gray-Level Histograms", *IEEE Trans Syst Man Cybern*, Vol. SMC-9, No. 1, pp. 62–66, Jan. 1979.

[25] "Types of Morphological Operations - MATLAB & Simulink". https://www.mathworks.com/help/images/morphological-dilation-and-erosion.html (accessed Mar. 22, 2021).

[26] P. Soille, "Morphological image analysis: principles and applications," Springer Science & Business Media, 2013.

[27] R. Srisha and A. Khan, "Morphological Operations for Image Processing : Understanding and its Applications", *National Conference on VLSI, Signal provessing & communications*, pp. 17–19, December 19 2013.

[28] S. Albawi, T. A. Mohammed, and S. Al-Zawi, "Understanding of a convolutional neural network", *Proceedings of 2017 International Conference on Engineering and Technology, ICET 2017*, Vol. 2018-Janua, No. April 2018, pp. 1–6, 2018.

[29] T. F. Gonzalez, "Handbook of approximation algorithms and metaheuristics", *Handbook of Approximation Algorithms and Metaheuristics*, pp. 1–1432, 2007.

[30] A. Ardakani, C. Condo, M. Ahmadi, and W. J. Gross, "An Architecture to Accelerate Convolution in Deep Neural Networks", *IEEE Transactions on Circuits and Systems I: Regular Papers*, Vol. 65, No. 4, pp. 1349–1362, 2018.

[31] Y. Zhang, J. Gao, and H. Zhou, "Breeds Classification with Deep Convolutional Neural Network", *ACM International Conference Proceeding Series*, pp. 145–151, 2020.

[32] J. Wu, "Introduction to Convolutional Neural Networks", *Introduction to Convolutional Neural Networks*, pp. 1–31, 2017, [Online]. Available: https://web.archive.org/web/20180928011532/https://cs.nju.edu.cn/wujx/teaching/15_CNN.pdf.

[33] Raid Rafi Omar Al-Nima, "Signal Processing and Machine Learning Techniques for Human Verification Based on Finger Textures", PhD thesis, School of Engineering, Newcastle University, UK, 2017.

[34] H. Sinha, R. Manekar, Y. Sinha, and P. K. Ajmera, "Convolutional neural network-based human identification using outer ear images", *Advances in Intelligent Systems and Computing*, Vol. 817, pp. 707–719, 2019.

[35] M. Banzi, *Getting Started with Arduino, 2nd Edition - O'Reilly Media*. 2011.

[36] Y. A. Badamasi, "The working principle of an Arduino", *Proceedings of the 11th International Conference on Electronics, Computer and Computation, ICECCO 2014*, 2014.

[37] P. Kanani and M. Padole, "Real-time Location Tracker for Critical Health Patient

using Arduino, GPS Neo6m and GSM Sim800L in Health Care", *Proceedings of the International Conference on Intelligent Computing and Control Systems, ICICCS 2020*, No. Iciccs, pp. 242–249, 2020.

[38] SIMCom, "Sim800L_Hardware_Design_V1.00", *A company of Sim Tech*, pp. 1–70, 2013, [Online]. Available: http://wiki.seeedstudio.com/images/4/46/SIM800L_Hardware_Design_V1.00.pdf.

[39] R. R. O. Al-Nima, S. S. Dlay, W. L. Woo, and J. A. Chambers, "Efficient Finger Segmentation Robust to Hand Alignment in Imaging with Application to Human Verification", *5th IEEE International Workshop on Biometrics and Forensics (IWBF)*, 2017.

[40] Marwa MohamedSheet AL-Hatab, Raid Rafi Omar Al-Nima, Ilaria Marcantoni, Camillo Porcaro, and Laura Burattini, "Classifying Various Brain Activities by Exploiting Deep Learning Techniques and Genetic Algorithm Fusion Method", *TEST Engineering & Management*, Vol. 83, pp. 3035-3052, 2020.

[41] Marwa MohamedSheet AL-Hatab, Raid Rafi Omar Al-Nima, Ilaria Marcantoni, Camillo Porcaro, and Laura Burattini, "Comparison Study Between Three Axis Views of Vision, Motor and Pre-Frontal Brain Activities", *Journal of Critical Reviews*, Vol. 7, Issue 5, pp. 2598-2607, 2020.

[42] Raid Rafi Omar Al-Nima, Saba Qasim Hasan, and Sahar Esmail, "Exploiting the Deep Learning with Fingerphotos to Recognize People", *International Journal of Advanced Science and Technology*, Vol. 29, No. 7, pp. 13035 – 13046, 2020.

[43] Lubab H. Albak, Raid Rafi Omar Al-Nima, and Arwa Hamid Salih, "Palm print Verification Based Deep Learning", *TELKOMNIKA Telecommunication, Computing, Electronics and Control*, Vol. 19, No. 3, 2021.

[44] Musab T. S. Al-Kaltakchi, Raid Rafi Omar Al-Nima, Mahmood Alfathe, and Mohammed A. M. Abdullah, "Speaker Verification Using Cosine Distance Scoring with i-vector Approach", in *2020 International Conference on Computer Science and Software Engineering (CSASE)*, IEEE, 2020.

[45] Musab T. S. Al-Kaltakchi, Raid R. O. Al-Nima, and Mohammed A. M. Abdullah, "Comparisons of extreme learning machine and backpropagation-based i-vector approach for speaker identification", *Turkish Journal of Electrical Engineering & Computer Sciences*, The Scientific and Technological Research Council of Turkey, Vol. 38, No. 3, pp. 1236-1245, 2020.

[46] R. R. Al-Nima and F. S. Mustafa, "Face Recognition Using Invariant Moments Features", *The Scientific Journal, College of Science, Tikrit University, Salahadeein, Iraq*, Vol. 14, No. 2, 2009.

[47] M. R. Khalil, M. S. Majeed, and R. R. Omar, "Personal Identification With Iris Patterns", *AL-Rafidain Journal of Computer Sciences and Mathematics, College of Computer Sciences and Math / University of Mosul / Iraq*, Vol. 6, No. 1, 2009.

[48] Raid R. O. Al-Nima, Tingting Han, Taolue Chen, Satnam Dlay, and Jonathon Chambers, "Finger Texture Biometric Characteristic: a Survey", *arXiv preprint arXiv:2006.04193*, 2020.

[49] R. R. O. Al-Nima, N. A. Al-Obaidy, and L. A. Al-Hbeti, "Segmenting Finger Inner Surface for the Purpose of Human Recognition", *2nd International Conference on Engineering Technology and its Applications (IICETA)*, IEEE, pp. 105-110, 2019.

[50] Shaima Miqdad Mohamed Najeeb, Raid Rafi Omar Al-Nima, and Mohand Lokman Al-Dabag, "Reinforced Deep Learning for Verifying Finger Veins", *International Journal of Online and Biomedical Engineering (iJOE)*, Vol. 17, No. 07, pp. 19-26, July 2021. https://doi.org/10.3991/ijoe.v17i07.24655

[51]   Moatasem Yaseen Al-Ridha, Ammar Sameer Anaz, Raid Rafi Omar Al-Nima, "Expecting Confirmed and Death Cases of COVID-19 in Iraq by Utilizing Backpropagation Neural Network", *Bulletin of Electrical Engineering and Informatics*, Vol. 10, No. 4, pp. 2137-2143, August 2021.

[52]   Raid Rafi Omar Al-Nima, Tingting Han, Saadoon Awad Mohammed Al-Sumaidaee, Taolue Chen, and Wai Lok Woo, "Robustness and performance of Deep Reinforcement Learning", *Elsevier, Applied Soft Computing*, Vol. 105, 2021.

[53]   Raid R. Al-Nima, Fawaz S. Abdullah, and Ali N. Hamoodi, "Design a Technology Based on the Fusion of Genetic Algorithm, Neural Network and Fuzzy Logic", *arXiv:2102.08035*, 2021.

[54]   Arwa Hamed Salih Hamdany, Raid Rafi Omar Al-Nima, and Lubab H. Albak, "Translating cuneiform symbols using artificial neural network", *TELKOMNIKA Telecommunication, Computing, Electronics and Control*, Vol. 19, No. 2, pp. 438~443, 2021.

[55]   Raid Rafi Omar Al-Nima, Muhammed Khidr Jarjes, Ahmed Waled Kasim, and Sinan S. Mohammed Sheet, "Human Identification using Local Binary Patterns for Finger Outer Knuckle", In *2020 IEEE 8th Conference on Systems, Process and Control (ICSPC)*, Melaka, Malaysia, pp. 7-12, 2020.

[56]   Ammar Sameer Anaz, Raid Rafi Omar Al-Nima, and Moatasem Yaseen Al-Ridha, "Multi-Encryptions System Based on Autoencoder Deep Learning Network", *Solid State Technology*, Vol. 63, Issue 6, 2020.

[57]   Wai Lok Woo, Bin Gao, Raid Rafi Omar Al-Nima, and Wing-Kuen Ling, "Development of Conversational Artificial Intelligence for Pandemic Healthcare Query Support", *International Journal of Automation, Artificial Intelligence and Machine Learning*, Vol. 1, Issue 1, 2020.

[58]   Mabroukah M. A. Abuqadumah, Musab A. M. Ali, and Raid R. O. Al-Nima, "Personal Authentication Application Using Deep Learning Neural Network", in *16th IEEE International Colloquium on Signal Processing & its Applications (CSPA)*, Langkawi, Malaysia, pp. 186-190, 2020.

[59]   Lubab H. Albak, Arwa Hamed, and Raid Rafi Omar Al-Nima, "Design Security System based on Arduino", *TEST Engineering & Management*, The Mattingley Publishing Co., Inc., Vol. 82, pp. 3341-3346, January-February 2020.

[60]   Arwa Hamid Salih Hamdany, Lubab H. Albak, and Raid Rafi Omar Al-Nima, "Wireless Waiter Robot", *TEST Engineering & Management*, The Mattingley Publishing Co., Inc., Vol. 81, pp. 2486-2494, November-December 2019.

[61]   Moatasem Yaseen Al-Ridha, Raid Rafi Omar Al-Nima, and Ammar Sameer Anaz, "Adaptive Neuro-Fuzzy Inference System for Controlling a Steam Valve", *in 2019 IEEE 9th International Conference on System Engineering and Technology (ICSET)*, Shah Alam, Malaysia, 2019.

[62]   R. R. O. Al-Nima, T. Han, and T. Chen, "Road Tracking Using Deep Reinforcement Learning for Self-driving Car Applications", In: R. Burduk, M. Kurzynski and M. Wozniak (eds), *Progress in Computer Recognition Systems, CORES 2019, Advances in Intelligent Systems and Computing*, Vol. 977, Springer, Cham, 2020.

[63]   F. M. Shehab, R. R. O. Al-Nima, and R. Y. Sedik, "Estimating Reference Evapo-Transpiration in Mosul (Iraq) Using Cascade Neural Networks", *Eng. & Tech. Journal*, Vol. 32, No. Part (A) 9, 2014.

[64]   Raid Rafi Al-Nima, "Steganography for Text in Video File Using Radial Neural Network", *3rd International Scientific Conference*, Foundation of Technical Education, Technical Education, Najaf, 2013.

[65] J. H. Al-Khalidy and R. R. Al-Nima, "Breast Tumor Classification Using SVM", *Tikrit Journal of Engineering Sciences*, Vol. 20, No. 5, 2013.

[66] D. A. B. Keryou, R. R. Al-Nima, and R. N. Wadie, "Design of Beam-Columns Using Artificial Neural Networks", *Eng. & Tech. Journal*, Vol. 30, No. 16, 2012.

[67] Ali Al-Askery, Charalampos C. Tsimenidis, Said Boussakta, and Jonathon A. Chambers, "Improved coded massive MIMO OFDM detection using LLRs derived from complex ratio distributions", In *2015 IEEE 20th International Workshop on Computer Aided Modelling and Design of Communication Links and Networks (CAMAD)*, pp. 64-68, IEEE, 2015.

[68] Ali J. Al-Askery, Charalampos C. Tsimenidis, and Said Boussakta, "Fixed-point arithmetic detectors for massive MIMO-OFDM systems", In *2015 23rd European Signal Processing Conference (EUSIPCO)*, pp. 919-923. IEEE, 2015.